Nonlinear LS-RTM based on the seismic scale separation and full wavefield multi-parameter FWI

Øystein Korsmo, Yang Yang, Nizar Chemingui, Andrey Pankov and Antonio Castiello, PGS*

Summary

Least-squares migration (LSM) images the subsurface through an inversion process and seeks the reflectivity model that best explains the measured data. This data-fitting process will implicitly compensate for wavefield propagation effects and limited resolution seen with conventional imaging. These favourable properties have made it the method of choice in complex geological settings.

In this paper, we will discuss the various properties and implementations of LSM and Full Waveform Inversion (FWI) and suggest a new nonlinear least-squares reverse time migration (LS-RTM) implemented in the framework of FWI. The new inversion estimates the earth reflectivity while updating the velocity model at every iteration. We demonstrate the new solution on a field data example from the Norwegian Sea.

Introduction

LSM is a linear inversion process with a convex objective function. It updates the reflectivity by matching the high wavenumber perturbations in the observed and synthetic data (Nemeth *et al*., 1999). The linear property of the inversion relates to the fixed background model, meaning that the velocity field is assumed known and kept unchanged during the inversion, making it feasible to estimate with a linear solver (Gauthier *et al*., 1986; Mora, 1989). The synthetic data are generated based on the Born approximation, where only the first order scattering term is utilized in the forward modeling step (Woodhouse, 1980; Tanimoto, 1984). In practice, this means that only the near- to mid-reflection angles can be utilized in the inversion process.

On the other hand, FWI is a highly nonlinear inversion with a complex objective function consisting of many local minima (Tarantola, 1987). The aim of FWI is to minimize the misfit between observed and modeled data. To linearize the inversion, the model parameters can be updated with a gradient descent approach that utilizes smaller steps in combination with a multi-stage process. In practice, this means that the lowest frequencies are first used and matched before higher frequencies are included in the inversion, to reveal more details in the model. FWI is commonly implemented with the adjoint-state method (Chavent, 1974), where the adjoint states refer to the backpropagated data-residuals and the gradient of the least-squares misfit is a migration operator (Lailly, 1983; Tarantola, 1984). Refractions and diving waves have proven to be robust and straightforward to utilize in FWI and have become the basis of most velocity model building projects. FWI can as well incorporate reflections, which allow velocity estimation beyond the penetration depth of diving waves. For this to be feasible, the modeling engine has to initiate the complete wavefield; diving waves, refractions and reflections (beyond Born approximations). In Figure 1, we show a comparison between Born modeling (a) and the full wavefield modeling (b). Notice that only the near to mid offsets/angles are generated with the Born approximation, while the full wavefield modeling generates the head-wave (yellow arrow) and diving waves/refractions (white arrow) in addition to low and high angle reflections.

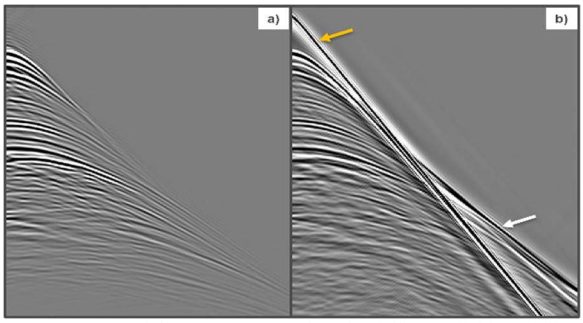

Fig 1: Born modeling (a) compared to the full wavefield modeling (b). The head-wave (yellow arrow), diving waves/refractions (white arrow) in addition to the full reflection angle range are only generated with the full wavefield modeling.

To make use of the complete wavefield, not limited by Born modeling, we propose a new nonlinear seismic inversion process, built on the FWI framework. The method can be considered as a multi-parameter FWI, where each model will be updated simultaneously without parameter-leakage. This can be achieved with a unique imaging condition, that naturally honours the seismic scale separation, and solve for the background model (velocities) and the perturbations (reflectivity) separately. The background model can be interpreted as the FWI long-wavelength velocities and the reflectivity can be described as a nonlinear LS-RTM, implemented with the adjoint state method. To handle the nonlinearity of this inversion, we follow the multi-stage approach until the background model reach convergence. From this point, we can perform large steps in frequency with the focus primarily on the reflectivity model.

The new implementation has been tested on a dataset over the recent 'Slagugle discovery' in PL-891, located 14 miles from the Heidrun field in the Norwegian Sea. The water depth is between 300-400 meters and the geology is characterized by heavily rotated fault blocks with large lateral velocity variations.

Methodology

Different implementations of LSM exist in both the image and data space, with curvelet domain matching filters, Point Spread Functions (PSFs) and the full iterative LSM (Guitton, 2004; Valenciano, 2008; Lu *et al*., 2017). Existing solutions include both ray-based and wave-theoretic migrations (Korsmo *et al*., 2019, 2021). A fundamental requirement is that the velocity model is assumed to be known and unchanged during the inversion. Errors in the velocity model may lead to instability issues and noisy results for the data-domain approach (Wang *et al*., 2021), as well as sub-optimal amplitude corrections with the image-domain implementation. To mitigate the kinematic misalignments due to an imperfect velocity model, a warping step prior or during the data-domain LSM, can be a pragmatic solution to stabilize the inversion (Luo *et al*., 2014). This approach will not focus the energy at the correct location in the sub-surface since the observed data gets shifted to the modeled data. A desired solution would be to refine the velocity model while inverting for the reflectivity. To achieve this, a natural approach would be to take a closer look at FWI, since RTM and FWI share the same modeling/migration engine and sensitivity kernels. The RTM/FWI sensitivity kernel consists of three different components; the "banana" related to the diving waves, the "rabbit ears" generated by reflections, and the migration isochrones. The first two contribute to the tomography kernel while the latter can be described as the impedance or reflectivity kernel.

Recent work has shown that FWI, with the access to modern compute resources, can be extended to high frequencies. The final high-resolution velocity model can post-inversion be converted to pseudo-reflectivity through a simple structural derivation step (Zhang *et al*., 2020; Kalinicheva *et al*., 2021). This approach will essentially leak reflectivity into the velocity model when implemented using a conventional cross-correlation imaging condition. Even when a density model is employed, it only acts as a passive parameter during FWI, and all reflectivity changes are simply mapped as velocity updates. Figure 2 shows how such an approach can introduce an incorrect velocity perturbation when the reflectivity is driven by the density contrast, not the velocity.

To reduce this parameter leakage, we make use of an alternative approach to keep the background model and the reflectivity separated and update them simultaneously during the inversion process (Yang *et al*., 2021). This can be achieved by separating the tomography from the reflectivity kernel using Inverse Scattering Imaging Condition during the inversion process (Whitmore and Crawley 2012; Ramos-Martinez *et al*., 2016). The process will isolate the tomographic kernel from the reflectivity kernel and use it to update the background model, which controls the kinematics and structural imaging. On the other hand, the reflectivity kernel will only contain the migration isochrones, and will be used to update the LS-RTM by matching the amplitudes between observed and modeled data. In order to utilize the full acoustic wavefield to update the velocity and reflectivity models, our solution utilizes an alternative formulation of the wave-equation, based on vector reflectivity modeling, to simulate all acoustic wave modes observed in the data (Whitmore *et al*., 2020).

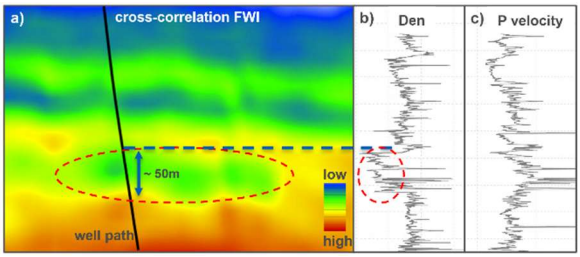

Figure 2: FWI velocity model from cross-correlation FWI where an incorrect (simple) density model was used as a passive parameter in FWI. The inversion detects an incorrect velocity decrease at the reservoir, caused by the strong change in reflectivity dominated by the drastic change in density.

Field data example

The new nonlinear data-domain LS-RTM was tested on a field data example from the Norwegian Sea over the 'Slagugle discovery'. We used a vintage velocity model and a fully pre-processed data for the test. The inversion can also be performed using raw data that includes free-surface multiples. By setting proper boundary conditions, the forward modeling engine can generate synthetic data that is consistent with the input field data for either scenario. When using raw data, the multiples crosstalk generated by the imaging of multiples can, in principle, be attenuated by the iterative inversion process (Lu *et al*., 2018).

To handle the nonlinear property of this seismic inversion, the process was done in frequency stages. Figure 3 shows three different frequency panels with the interleaved (observed and modeled data) after the 25 Hz inversion. The kinematic alignment indicates that the background model has been resolved.

In figure 4a-b, we show comparison of the 25 Hz initial (RTM) and updated nonlinear LS-RTM. The corresponding FK-spectra and amplitude spectrum are shown in figure 4c-e, where the nonlinear LS-RTM clearly broadens the wavenumber content both laterally and vertically. The inverted reflectivity shows a much-improved image, with a balanced amplitude response, enhanced resolution, and improved fault imaging.

Jointly with the reflectivity updates, a refinement of the velocity model was achieved. Figure 5a shows the accumulated velocity perturbation and 5b shows the angle gathers from wave-equation migration. The flatness of the angle gathers, from the refined velocity model, indicate a well resolved background trend and further support the data domain QC in figure 3. Notice that the velocity perturbations are structurally consistent, and the updates penetrate to the full image range (where there is reflectivity in the image). This was made possible by utilizing the full seismic wavefield in the inversion process, including reflections.

In addition to the kinematic alignments shown in figure 3 (related to the background model) the inversion will suppress the data-residuals and amplitude effects caused by high wavenumber scattering (explained by the reflectivity model). Figure 6 show the data-domain QC for a single shot gather in the middle of the cross-section. The observed data is shown in 6a, the modeled data with initial model compared to the updated one are in 6b-c and the corresponding data-residuals in 6d-e. The updated reflectivity and velocity clearly improve the data-match and result in reduced data-residuals as annotated by the arrows.

After we obtained convergence at 25 Hz, the highly nonlinear nature of the inversion will become more linear, meaning that further iterations at higher frequencies will lead to only small perturbations in the background model. This argument justifies larger frequency steps once the background model has been resolved. After the 25 Hz inversion, we took a big step in frequency and continued the inversion at 45 Hz, mainly focusing on the reflectivity model. Figure 7 shows the nonlinear LS-RTM at 25 and 45 Hz. As expected, the increase in frequency reveals further details and increased resolution in the image.

Conclusions

We have demonstrated how our new nonlinear data-domain LS-RTM, implemented using the adjoint state method, can invert for the reflectivity while simultaneously refining the FWI velocity model. This mitigates the need to stabilize the data-domain LSM with a warping process. The implementation takes advantage of the similarities between RTM and FWI and our unique imaging condition to carefully update the velocity and reflectivity without any leakage between the two models. In particular, reflectivity changes caused by density variations are not erroneously mapped as velocity updates. The inversion utilizes the full acoustic wavefield through an alternative formulation of the wave-equation parametrized in terms of velocity and vector reflectivity. The nonlinear LS-RTM results show significant structural improvements, more focusing, and better fault imaging compared to the RTM.

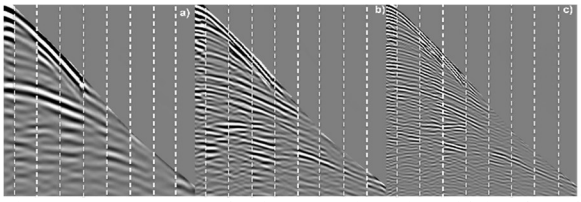

Figure 3: Frequency panels after 25 Hz inversion with interleaved shots (observed/modeled), separated by the vertical dotted lines, 4-7Hz (a), 7-15 Hz (b) and 15-30 Hz (c). The kinematic alignment indicates that the background model has been well resolved.

Acknowledgements

We thank PGS for the permission to present this work and AkerBP for allowing us to use their data example in figure 2.

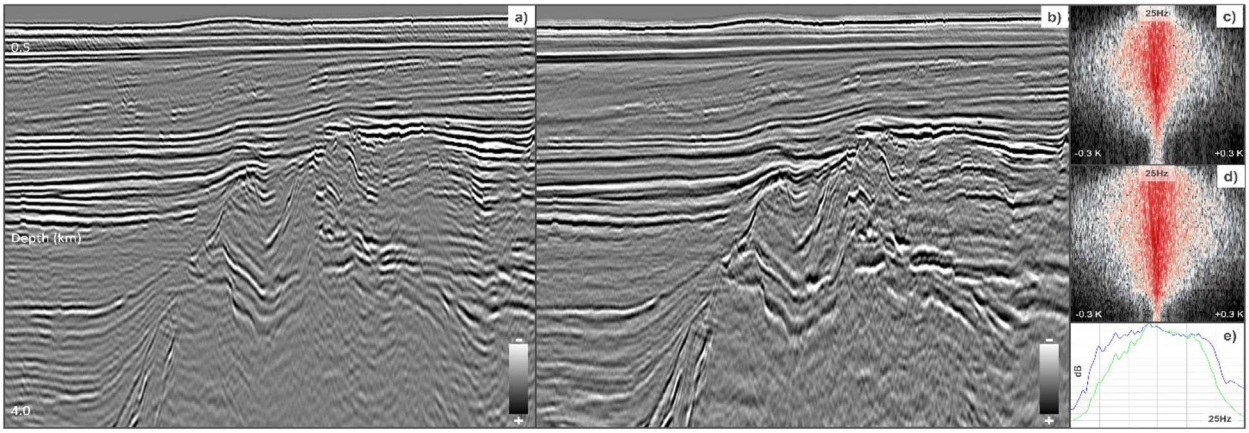

Figure 4: Comparison of RTM (a) and the new data-domain LS-RTM (b) with the corresponding FK-spectra in (c) and (d). Comparison of the amplitude spectra are shown in (f), where the green curve corresponds to RTM and the blue curve shows the LS-RTM. Notice the improvements in the wavenumber content, amplitude fidelity, structural imaging and fault mapping in the LSRTM results compared to the RTM.

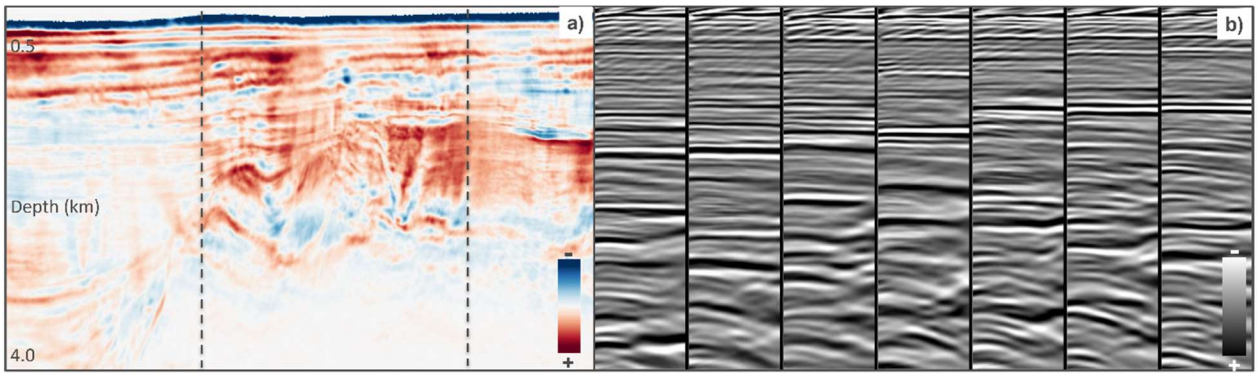

Figure 5: Accumulated velocity difference with +/- 100m/s display range (a) and imaging QC of the refined velocity model through the centre of the line, between the two stipulated lines (b). The velocity updates are structurally consistent with the image and produce flat angle gathers computed with wave-equation migration.

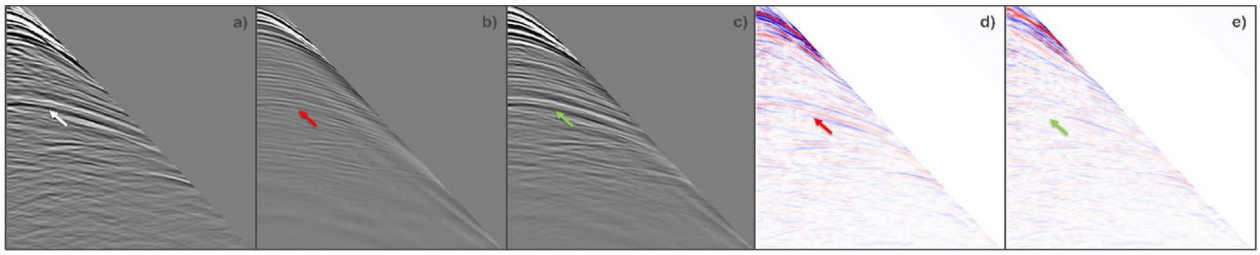

Figure 6: Recorded shot gather after full pre-processing (a), synthetic data with the initial reflectivity/velocity models (b) and with updated models (c) and the corresponding initial (d) and updated data-residuals (e). Notice the improved data-match after inversion and the reduction in the data-residuals after inversion, as annotated by the arrows.

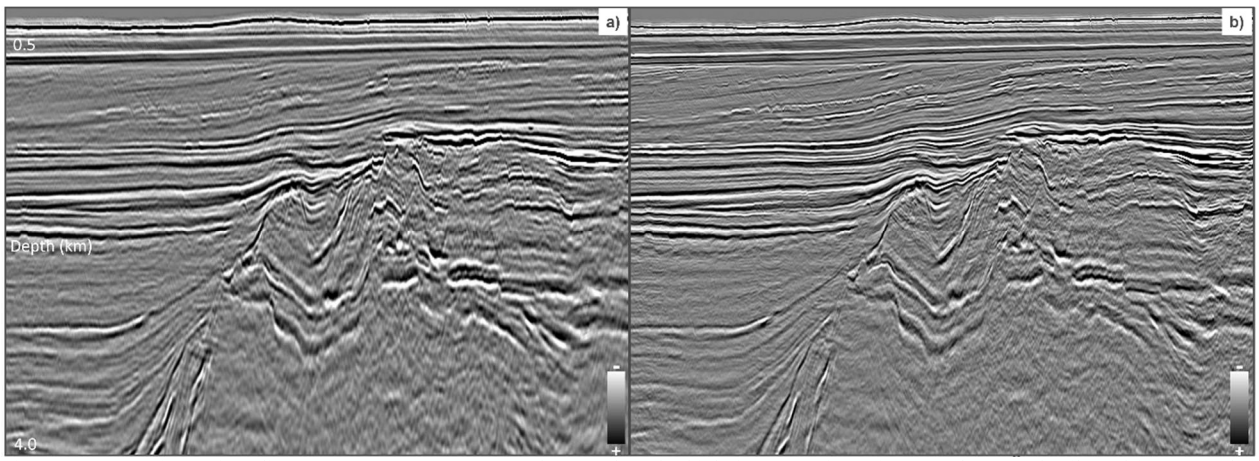

Figure 7: Comparison of nonlinear LS-RTM at 25Hz (a) and 45Hz (b). The high frequency inversion reveals more details and improves the resolution in the image.

REFERENCES

Chavent, G., 1974, Identification of function parameters in partial differential equations: Presented at the Joint Automatic Control Conference.

Gauthier, O., J. Virieux, and A. Tarantola, 1986, Two-dimensional nonlinear inversion of seismic waveforms: Numerical results: Geophysics, **51**, 1387–1403, doi: https://doi.org/10.1190/1.1442188.

Guitton, A., 2004, Amplitude and kinematic corrections of migrated images for nonunitary imaging operators: Geophysics, **69**, no. 4, 1017–1024, doi: https://doi.org/10.1190/1.1778244.

Kalinicheva, T., M. Warner, and F. Mancini, 2021, Full-bandwidth FWI: 82nd Annual International Conference and Exhibition, EAGE, Extended Abstracts.

Korsmo, Ø., S. Arasanipalai, and Z. Greplowsk, 2019, Application of iterative least-squares migration in different geological settings: 81st Annual International Conference and Exhibition, EAGE, Extended Abstracts.

Korsmo, Ø., C. Crawley, C. Zhou, S. Lee, E. Klochikhina, and N. Chemingui, 2021, Least-squares Kirchhoff PSDM with a local based inversion approach and compensation for limitations in modeling: 82nd Annual International Conference and Exhibition, EAGE, Extended Abstracts.

Laily, P., 1983, The seismic inverse problem as a sequence of before stack migration: Presented at the Proceedings of Conference on Inverse Scattering, Theory and Applications, SIAM Philadelphia, Pennsylvania.

Lu, S., X. Li, A. Valenciano, N. Chemingui, and C. Cheng, 2017, Least-squares wave-equation migration for broadband imaging: Presented at the 79th Annual International Conference and Exhibition, EAGE, Extended Abstracts.

Lu, S., F. Liu, N. Chemingui, and M. Orlovich, 2018, Full wavefield migration by inversion. Presented at the SEG Technical Program Expanded Abstracts, 4311–4315.

Mora, P., 1989, Inversion = migration + tomography: Geophysics, **54**, 1575–1586, doi: https://doi.org/10.1190/1.1442625.

Nemeth, T., C. Wu, and G. T. Schuster, 1999, Least-squares migration of incomplete reflection data: Geophysics, **64**, no. 1, 208–221, doi: https://doi.org/10.1190/1.1444517.

Ramos-Martinez, J., S. Crawley, Z. Zou, A. A. Valenciano, L. Qui, and N. Chemingui, 2016, A robust gradient for long wavelength FWI updates: 78th Annual International Conference and Exhibition, EAGE, Extended Abstracts.

Tanimoto, T., 1984, A simple derivation of the formula to calculate synthetic long-period seismograms in a heterogeneous Earth by normal mode summation: Geophysical Journal International **77**, 275–278, doi: https://doi.org/10.1111/j.1365-246X.1984.tb01934.x.

Tarantola, A., 1984, Linearized inversion of seismic reflection data: Geophysical Prospecting, **32**, 998–1015, doi: https://doi.org/10.1111/j.1365-2478.1984.tb00751.x.

Tarantola, A., 1987, Inverse Problem theory, methods for data fitting and model parameter estimation: Elsevier.

Valenciano, A. A., 2008, Imaging by wave-equation inversion: PhD thesis, Stanford University.

Wang, B., Y. He, J. Mao, F. Liu, F. Hao, Yi. Huang, M. Perz, and S. Michell, 2021, Inversion-based imaging: from LSRTM to FWI imaging: First Break, 85–93.

Whitmore, N. D., and S. Crawley, 2012, Application of RTM inverse scattering imaging conditions: 82nd Annual International Meeting, SEG, Expanded Abstracts, doi: https://doi.org/10.1190/segam2012-0779.1

Woodhouse, J., 1980, The coupling and attenuation of nearly resonant multiples in the Earth free oscillation spectrum: Geophysical Journal International, **61**, 261–283, doi: https://doi.org/10.1111/j.1365-246X.1980.tb04317.x.

Yang, Y., J. Ramos-Martinez, G. Huang, D. Whitmore, and N. Chemingui, 2021, Simultaneous velocity and reflectivity inversion: FWI + LSRTM: 82nd Annual International Conference and Exhibition, EAGE, Extended Abstracts.